MATERIALS SCIENCE

Morphing pasta and beyond

Ye Tao[1,2,3], Yi-Chin Lee[4], Haolin Liu[5], Xiaoxiao Zhang[6†], Jianxun Cui[1], Catherine Mondoa[7], Mahnoush Babaei[5], Jasio Santillan[7], Guanyun Wang[3], Danli Luo[1], Di Liu[6], Humphrey Yang[1], Youngwook Do[1,8], Lingyun Sun[3], Wen Wang[1]*‡, Teng Zhang[6,9]*, Lining Yao[1,5]*

Morphing structures are often engineered with stresses introduced into a flat sheet by leveraging structural anisotropy or compositional heterogeneity. Here, we identify a simple and universal diffusion-based mechanism to enable a transient morphing effect in structures with parametric surface grooves, which can be realized with a single material and fabricated using low-cost manufacturing methods (e.g., stamping, molding, and casting). We demonstrate from quantitative experiments and multiphysics simulations that parametric surface grooving can induce temporary asynchronous swelling or deswelling and can transform flat objects into designed, three-dimensional shapes. By tuning the grooving pattern, we can achieve both zero (e.g., helices) and nonzero (e.g., saddles) Gaussian curvature geometries. This mechanism allows us to demonstrate approaches that could improve the efficiency of certain food manufacturing processes and facilitate the sustainable packaging of food, for instance, by creating morphing pasta that can be flat-packed to reduce the air space in the packaging.

INTRODUCTION

The plastic material used in food packaging, is a major contributor to landfills in the United States (*1*). Finding effective food packaging strategies is crucial to maintaining a sustainable future. Researchers have proposed the design concept of "morphing" food that can be flat-packed to reduce packing space during transportation and storage (*2*, *3*). Taking pasta as an example, although three-dimensional (3D) pasta is widely known for its unique texture, mouth feel, and pairing with different sauces, it takes up more space than flat pasta when packaged and becomes more fragile during transportation. Flat-packed 3D pasta may, therefore, be a possibility if a suitable morphing mechanism can be developed that enables flat pasta to morph into the target 3D shapes during cooking. However, many existing morphing mechanisms cannot be applied practically to morphing food, such as those relying on structural anisotropy (*4*–*7*), material composition (*8*–*12*), or composite bilayers and hinges (*13*–*18*), as these create mismatch strains within the materials. With regard to food, material composition is subject to many constraints, associated with nutritional requirements or culinary culture. For example, authentic Italian pasta dough is only supposed to be made of semolina flour and water. In addition, restrictions are also placed on manufacturing techniques due to cost and food safety. To fulfill these functional requirements, the generation of surface grooves has been introduced for morphing flour-based food, since this works with a single material and simple manufacturing method (*3*). However, the previous study did not explain the underlining morphing mechanism and relied heavily on experimental trial and error for the morphing design. The lack of quantitative design and analysis hinders the development of a comprehensive guiding design principle. Furthermore, the designed samples were limited to simple geometries with zero Gaussian curvatures.

Outside the context of food, interest has been shown in investigating the diffusion-based mechanism for morphing (*19*–*24*). In particular, surface groove–induced morphing has recently been reported in 3D-printed hydrogels. A simplified bilayer model (*20*) and the effect of surface area–to–volume ratio on the swelling ratio (*19*) were used to explain the morphing mechanism. However, the transient nature of asymmetrical swelling in 3D structures is not fully understood. In our experiments, we observe that the morphing caused by surface grooves is temporary, with the morphing structure eventually swelling fully and flattening again (at 470 s; see Fig. 1A). Our modeling of the kinetic swelling process at the level of individual grooves confirms that a delayed response to stimuli (exposure to a solvent or air) for the center of protrusions, compared to other regions (e.g., top or bottom of the surface exposed), causes asymmetrical morphing of the object, as illustrated in Fig. 1B. Understanding the transient nature of morphing during swelling is crucial to our design strategy, as we can either leverage it to create bidirectional and reversible actuation, exemplified by polydimethylsiloxane (PDMS) samples (Fig. 1A), or purposely introduce a groove-fusing process to lock the morphed structures and make their transformation nonreversible (as shown in the pasta samples; see Fig. 1C). Furthermore, through tightly coupled large-scale finite element (FE) simulations and quantitative experiments, we confirm that groove parameters (e.g., side angle, gap, width, and depth) affect the kinetics of diffusion and the morphing behaviors, which become critical design parameters.

To demonstrate the relevance of such a mechanism and the potential application to morphing food, flour dough (a material composed of starch granules and a gluten network), a typical easy-to-access material found in most kitchens, is selected. By creating simple surface grooves, the morphing of the dough structure, governed by swelling, is achieved by cooking it in boiling water (movie S1). The making of the groove can easily be prototyped through low-cost manufacturing methods, such as stamping (fig. S1A), molding

[1]Human-Computer Interaction Institute, Carnegie Mellon University, Pittsburgh, PA, USA. [2]School of Artistic Design and Creation, Zhejiang University City College, Hangzhou, China. [3]College of Computer Science and Technology, Zhejiang University, Hangzhou, China. [4]Computational Design, School of Architecture, Carnegie Mellon University, Pittsburgh, PA, USA. [5]Department of Mechanical Engineering, Carnegie Mellon University, Pittsburgh, PA, USA. [6]Department of Mechanical and Aerospace Engineering, Syracuse University, Syracuse, NY, USA. [7]Department of Materials Science and Engineering, Carnegie Mellon University, Pittsburgh, PA, USA. [8]School of Interactive Computing, Georgia Institute of Technology, Atlanta, GA, USA. [9]BioInspired Syracuse, Syracuse University, Syracuse, NY, USA.
*Corresponding author. Email: wen.wang@rd.nestle.com (W.W.); tzhang48@syr.edu (T.Z.); liningy@andrew.cmu.edu (L.Y.)
†Present address: Anyang Institute of Technology, Anyang, China.
‡Present address: Nestlé R&D Center (Pte) Ltd., Singapore.

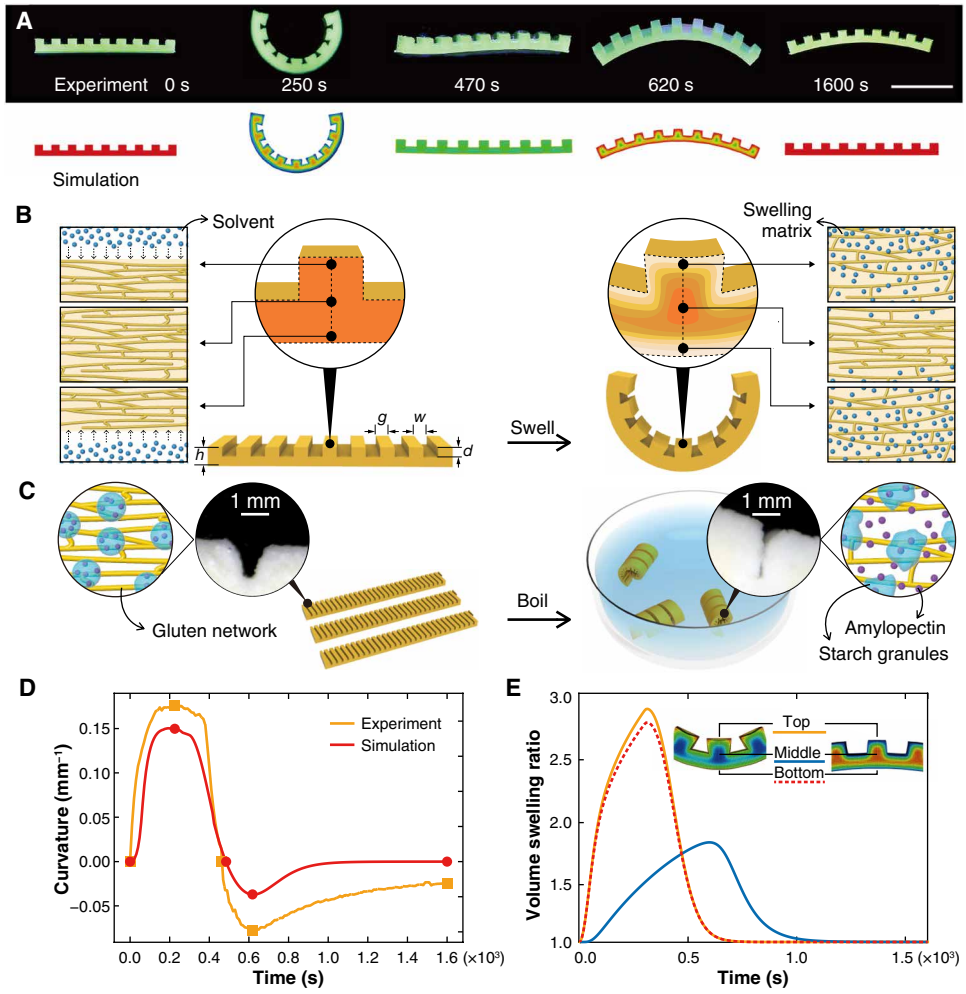

Fig. 1. Morphing mechanism and manufacturing process for pasta and silicone elastomer (PDMS). (**A**) Experimental and simulation results of swelling (in solvent) and deswelling (in air) of the grooved PDMS strips. The bending is transient, bidirectional, and reversible. (**B**) Schematic of the morphing mechanism caused by asymmetric surface grooves on the strip. The center of the protrusion having a slower swelling rate compared to the edges. The geometrical factors of the grooves include the groove width (*w*), gap (*g*), depth (*d*), and the total strip thickness (*h*). (**C**) Shape transformation of fusilli lunghi pasta (i.e., long spirals) before and after cooking. As the grooves collide, the pasta surfaces leak amylopectin, causing them to adhere to one another. (**D**) The changes of bending curvatures for the experiment and simulation of the PDMS strips in (A). (**E**) Simulation of volumetric swelling ratios in different regions of the PDMS strips in (A). The color in (A) represents the polymer volume fraction. Color bars have been omitted because the absolute values are not critical information.

and casting (fig. S1B), or laser etching (*25*), to accommodate the manufacturing limitations imposed in the food industry and to suit the needs of materials with different elastic or viscoelastic behaviors. The general design strategy introduced here could also potentially be applied to a broad category of food gels (*26*), since most food gels are hydrophilic gels and can undergo volumetric expansion induced by hydration during cooking.

In terms of the shapes that can be achieved through groove-based morphing, despite the variety previously shown (*3*, *20*), the majority were based on parallel lines of grooves with limited design guidelines. Here, we demonstrate a broadened shape space and design guidelines for helix-based geometries with parallel lines and cone frustum-based geometries with radial lines, and we describe more complicated morphing shapes by integrating the primitives (i.e., a single helix and cone frustum). We also present nonzero Gaussian curvature shapes, such as saddles and twists, by introducing double-sided grooves. These results indicate an even greater scope for groove-based morphing with an enriched shape space and an increased range of potential applications.

RESULTS

Morphing mechanism

To establish the morphing mechanism, we first studied the bending strips of PDMS (a model material widely studied in terms of its kinetic behaviors during diffusion processes) (*27*–*29*). The transformation was triggered by nonpolar solvent immersion (upward bending via swelling at 250 s; see Fig. 1A), followed by solvent evaporation in air (downward bending via deswelling at 620 s; see Fig. 1A). The grooved PDMS strips exhibited reversible and bidirectional morphing behaviors. Our simulations based on a polymeric gel model (*30*, *31*) could accurately predict the morphing

phenomenon and matched well with the experimental results (Fig. 1, A, D, and E, and movie S2), confirming that asynchronous diffusion between the center and other regions causes transient morphing of the object.

To verify that the same groove-based morphing mechanism of PDMS can be applied to flour dough, a disk-swelling test of both PDMS and pasta was conducted and simulated further via a numerical model (Fig. 2A). We integrated data from the disk-swelling test for the morphing sample simulation and found that the same polymeric gel model could be applied to explain the bending of both materials (bending PDMS strips as shown in fig. S2 and bending pasta strips as shown in Fig. 2B and fig. S3). The differences between the strip samples made of both materials, in terms of the bending time and bending curvature, were mainly caused by their unique material composition and physical properties, such as Young's modulus, the Flory-Huggins interaction parameter, and diffusion coefficient (the parameters used in both the PDMS and pasta samples are listed in table S1).

Capturing the morphing phenomenon across different materials (i.e., PDMS and pasta strips) with a uniform polymeric gel-based diffusion model is critical if we are to justify that the morphing is mainly due to geometrical factors. Although our pasta manufacturing and processing (e.g., stamping of the flour dough) may have introduced other changes in local material density and contact surface areas, the morphing phenomenon of the pasta samples could still be captured by the same groove-induced asynchronous diffusion model, validating our hypothesis that the geometrical grooves play a critical role in the pasta's morphing behavior.

Geometrical features of grooves

The geometrical features of grooves can influence morphing. We experimentally varied the parameters of the grooves for both the pasta and the PDMS strips (e.g., groove width, depth, gap, and base thickness) in the micrometer-to-millimeter range and observed that the strip samples morphed in a parametrically controllable manner (Fig. 2B and figs. S2 and S3). For example, the maximum bending curvature of the strips was found to increase as the groove width, depth, gap, and base thickness decreased. However, if the gap between neighboring grooves was small enough to cause collision of the grooves, then the structure did not bend any further, which was predicted in our simulation model and further validated in experiments on the PDMS strip sample with a groove width of 0.5 mm (shown in fig. S2).

In addition to its influence on the maximum bending angle, this collision of adjacent walls during morphing can be leveraged for shape-locking purposes in the case of flour dough [where leakage of amylopectin from starch granules during cooking functions as a natural glue (*32*, *33*) that can partially fuse colliding grooves] (Fig. 1C, fig. S4, and movie S3). Together with irreversible gluten denaturation (*34*) and starch gelatinization (*35*), the morphing of flour dough became irreversible after cooking compared with the PDMS. Even with a prolonged hydration time (2 hours at 90°C), the bending curvature of the dough only displayed a 20% decrease. This also explains the deviation of the experimental results from the model with the smallest gap (0.5 mm) for dough (Fig. 2B), where glued grooves may have altered the physical and diffusion conditions. By contrast, in the case of dough with larger gaps (1.5 to 2.5 mm) (also shown in Fig. 2B), there was no colliding-fusing effect, so the simulation accurately predicted the actual dough morphing behavior.

We also found that fine adjustment of the groove wall structure could notably influence the bending angle. For instance, by adjusting the tilting angle of the groove walls from a cuboid shape into a quadrilateral frustum shape in the simulation (Fig. 2C), the bending angle could be maximized, as the frustum-shaped grooves reduced wall collision in the case of the narrow grooves (e.g., 0.5 mm in width) which may otherwise have prevented the sample from further bending.

Design guidelines and analysis

To specify the design guidelines, we introduce two groove-patterning rules for shapes with zero Gaussian curvatures: one or multiple groups of parallel straight lines on one side of a substrate that can be explained by the helix-based model, presented in Fig. 3; and one or multiple groups of radial lines on one side of a substrate that can be explained by the conical frustum model in Fig. 4.

First, we analyzed and experimentally validated a helix-based model (Fig. 3) using PDMS to explain the designs with one group of parallel straight lines on one side of a substrate. Inspired by the helix generated from origami folding with inclined folding lines, we created an inclined groove with a variable angle, β, in a rectangular strip that was 80 mm in length (*L*) and 5 mm in width (*T*) (Fig. 3A).

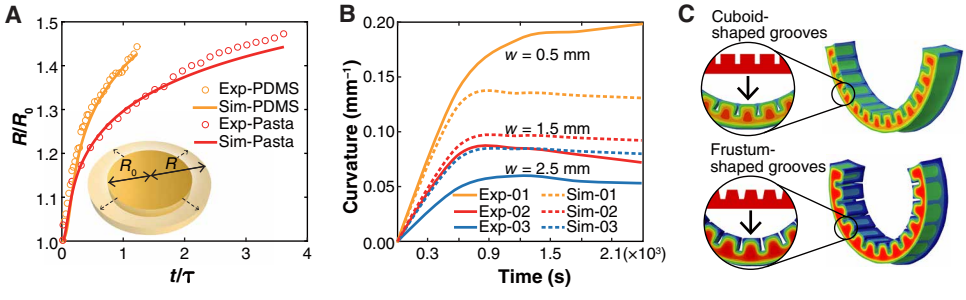

Fig. 2. Shared morphing mechanism between the strip samples of the PDMS and the flour dough with parametric grooves. (**A**) Measured and simulated radial swelling ratios (R/R_0) as a function of time (t) for pasta dough and silicone elastomer (PDMS) disks, where τ is the diffusion characteristic time scale of the disk. (**B**) Measured and simulated bending curvatures of pasta strips increased as the groove width (w) decreased. The bending self-locked and was not reversible. (**C**) Different bending curvatures of strips with cuboid and quadrilateral frustum-shaped grooves, from simulations of the PDMS strips of the same dimensions. Frustum-shaped grooves minimized the collision between neighboring grooves and thus increased the bending curvature. The color represents the polymer volume fraction. Color bars have been omitted because the absolute values do not constitute critical information.

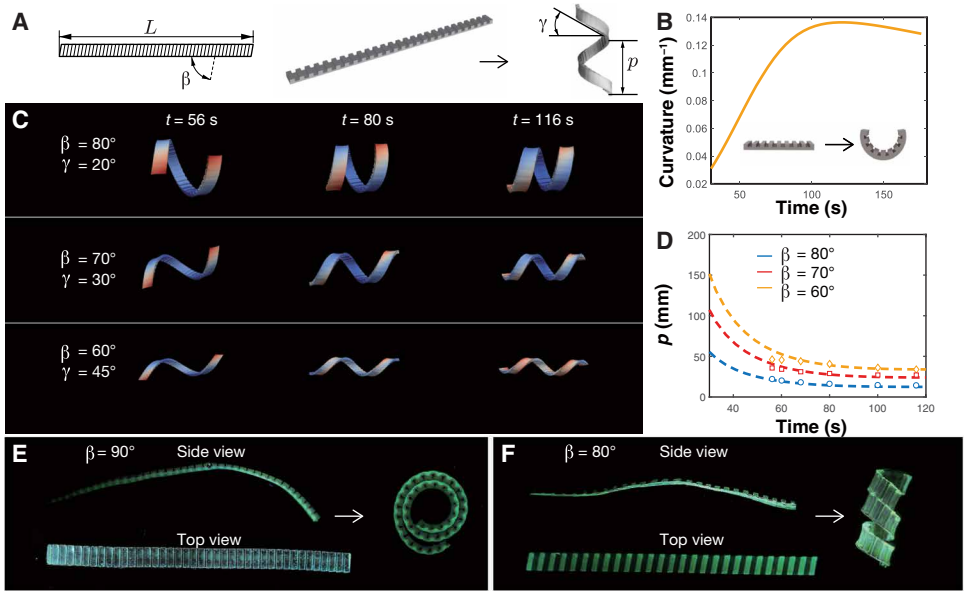

Fig. 3. Theoretical analysis and experimental validation of helix morphing during swelling. (**A**) Schematic of the helix morphing with parallel inclined groove patterns. (**B**) Simulated bending curvatures of a PDMS strip with $\beta = 90°$. (**C**) Simulated snapshots of the helix configurations of PDMS. The helix angle, γ, was measured from the simulation. (**D**) Simulated helix pitches for the PDMS strips with different inclined angles at different time points. The dotted data were measured from the simulations. (**E**) Bending configuration of a long PDMS strip ($L = 78.8$ mm). (**F**) A PDMS helix formed by a strip with inclined grooves ($L = 80.4$ mm). The groove pattern geometries in (A), (B), and (C) are $w = 1.0$ mm, $g = 1.5$ mm, $d = 0.75$ mm, and $h = 1.5$ mm. The groove geometry in (E) is $w = 0.5$ mm, $g = 1.5$ mm, $d = 1$ mm, and $h = 1.5$ mm, and the geometry in (F) is $w = 1.5$ mm, $g = 1.5$ mm, $d = 1$ mm, and $h = 1.5$ mm. The color in (C) represents the deformation magnitude. Color bars have been omitted because the absolute values are not critical information.

To predict the helix configurations (such as the number of helix loops, n, the helix pitch, p, and the helix angle, γ), we first simulated pure bending of the strip with the same grooves, except $\beta = 90°$ and the strip had a shorter length ($L = 21.5$ mm), from which we could obtain the curvature (κ_b) of the strip as a function of time (Fig. 3B). We then estimated the helix parameters based on the geometry model (*36*)

$$\bar{\gamma} = \frac{\pi}{2} - \beta, n = \frac{L\kappa_b}{2\pi}, p = \frac{2\pi}{\kappa_b}\sin\gamma \quad (1)$$

where $\bar{\gamma}$ is the ideal helix angle, assuming that most bending deformation occurs at the inclined lines. Equation 1 predicted that a full helix loop would form at time $t = 56$ s ($\kappa_b = 2\pi/(L) = 0.078$ mm^{-1}), which is confirmed by the simulated results shown in Fig. 3C. We found the helix angles, γ, in simulations, are different from the prediction, $\bar{\gamma}$, based on the geometry model and use the simulated value to calculate the helix pitch, p. As shown in Fig. 3D, the predictions for helix pitch, p, from the simple geometry model (dashed lines) were in good agreement with the simulations (marks). To guide the design more efficiently, it is of great importance to develop a scaling law for the helix angle, γ, in terms of groove geometries and material properties, and this will be reported in future studies. Figure 3 (E and F) shows two experimental samples with $L \approx 80$ mm, $T = 5$ mm, and varied angle, β. During the swelling process, the transformation in our experiments (movie S4) matched well with the prediction.

In addition to the helix-based model, straight radial grooves on an annulus sector were found to drive the structure to morph into an approximated conical frustum (Fig. 4). To understand this transformation, we performed some theoretical analyses based on a simple geometry model. As we checked the groove structures at different locations in the annulus sector (Fig. 4A), the key change was that the effective groove gap (g) varied. To quantify the effect of the groove gap on morphing, we systematically varied the groove gap in the straight PDMS strips from 1.5 to 6.5 mm and fixed other groove parameters ($w = 1$ mm, $d = 0.75$ mm, and $h = 1.5$ mm) and the strip width ($T = 5$ mm). As shown in Fig. 4B, the bending curvature (κ_b) was inversely proportional to the period of the groove ($g + w$)

$$\kappa_b = A(t)\frac{1}{g+w} \quad (2)$$

where $A(t)$ is a time-dependent parameter that can be obtained by fitting the numerical simulations. By noting $g + w = s\Delta\theta$, we can rewrite Eq. 2 as

$$\kappa_b = \frac{A(t)}{\Delta\theta}\frac{1}{s} \quad (3)$$

where $\Delta\theta$ is the angle period in the annulus sector, and s is the slant height. For the conical frustum, the nonzero principal curvature can be written as

$$\kappa_c = \tan(\alpha)\frac{1}{s} \quad (4)$$

where α is the cone angle. From a pure geometry point of view, we can establish a simple relationship between the cone angle, α, and the groove structures, by allowing $\kappa_b = \kappa_c$, which gives us

$$\tan(\alpha) = \frac{A(t)}{\Delta\theta} \quad (5)$$

Our full 3D simulations indeed showed that the structure would morph into an approximated conical frustum (Fig. 4C). Since the

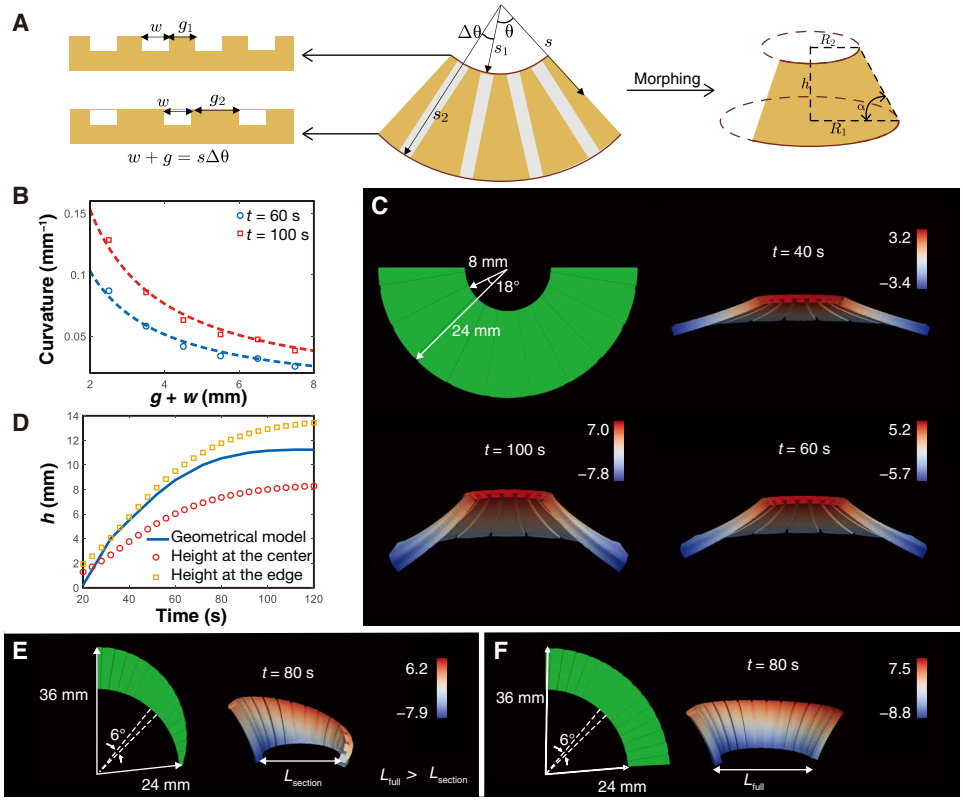

Fig. 4. Theoretical analysis of conical frustum morphing during swelling. (**A**) Schematic of the conical frustum morphing with radial groove patterns. The grooves have a fixed width and varied gaps at different radial locations. The angle of the annulus sector is θ_a. (**B**) Simulated bending curvatures of pasta strips with varying gaps (*g* is from 1.5 to 6.5 mm) and fixed width ($w = 1$ *mm*). (**C**) Simulated snapshots of the conical frustum configurations of PDMS at different times, formed by the annulus section. (**D**) Simulated and theoretical heights of the conical frustum of PDMS as a function of time. The dotted data were measured from simulations. (**E**) Morphing of a section of the conical frustum from a cut annulus sector, where the outer boundary is defined by circle passing points (0, 36), (24, 0), and (−24, 0). (**F**) Morphing of a conical frustum from the uncut annulus sector. The color bar represents the out-of-plane displacement (unit: millimeters) in (C), (E), and (F).

3D structure was not an ideal conical frustum, it was easier to compare the height in both simulations and geometrical analysis. In the geometrical model, we could compute the height as

$$h = (s_2 - s_1)\sin(\alpha) \quad (6)$$

where s_1 and s_2 are the radii of the inner and outer circles of the annulus sector. For the simulations, we measured the height at the center ($\theta = \theta_a/2$) and the edge ($\theta = 0°$) of the conical frustum, and these measurements were compared with our theoretical prediction (Fig. 4D). Here, θ_a is the angle of the annulus section. Overall, the simulated heights in Fig. 4D were in good agreement with the geometrical prediction, despite the model being highly simplified. The height at the edge is larger than the center because the side surface provides more solvent diffusion flux, to increase the swelling ratio. In addition, we found that a section of a conical frustum (Fig. 4E) could be formed through a cut annulus sector, following the same geometrical principle as a full conical frustum (Fig. 4F). More bending deformation occurred in the section of the conical frustum, which was probably due to the larger surface area–to–volume ratio.

Built on the conical frustum model, three PDMS samples were designed with the radial grooving pattern on designer-specified overall shapes (Fig. 5 and fig. S5). Whereas the rose flower (Fig. 5A and movie S5) and the cup (Fig. 5B and movie S6) were based on the full conical frustum model in Fig. 4, the frangipani flower pedal (Fig. 5C and movie S7) introduced an angled, conic section to the basic conical frustum model. In addition to the transformation during the swelling process, we observed that all three samples morphed toward the opposite side during deswelling, which matched our experiments and the simulations of the simple PDMS strips in Fig. 1A. These examples confirmed that simple surface grooving with a relatively low resolution (groove width, 0.5 to 1.5 mm) can serve as bidirectional, multistage, and reversible morphing mechanisms.

The same design principles were applied to design pasta morphing shapes with zero Gaussian curvatures (Fig. 6, A and B, and fig. S6, A and B). One or several groups of straight parallel grooves were used to design the samples in Fig. 6A, which could be explained by the helical model proposed in Fig. 3. Both the wing and ring shape in Fig. 6B could be explained by the conical frustum model from Fig. 4. In particular, the wing shape consisted of two groups of radial grooves on one side of the substrate. In the case of the ring, the four groups of radial grooves did not overlap one another, although two groups were on the opposite side to the others.

Nonzero Gaussian curvature pasta shapes can also be achieved (Fig. 6C and fig. S6C). Inspired by the rich morphing structures observed in a bilayer sheet with orthogonal shrinkages in the top and bottom layers, we designed pasta with double-sided and orthogonal grooves to form saddle and twist structures. While these examples

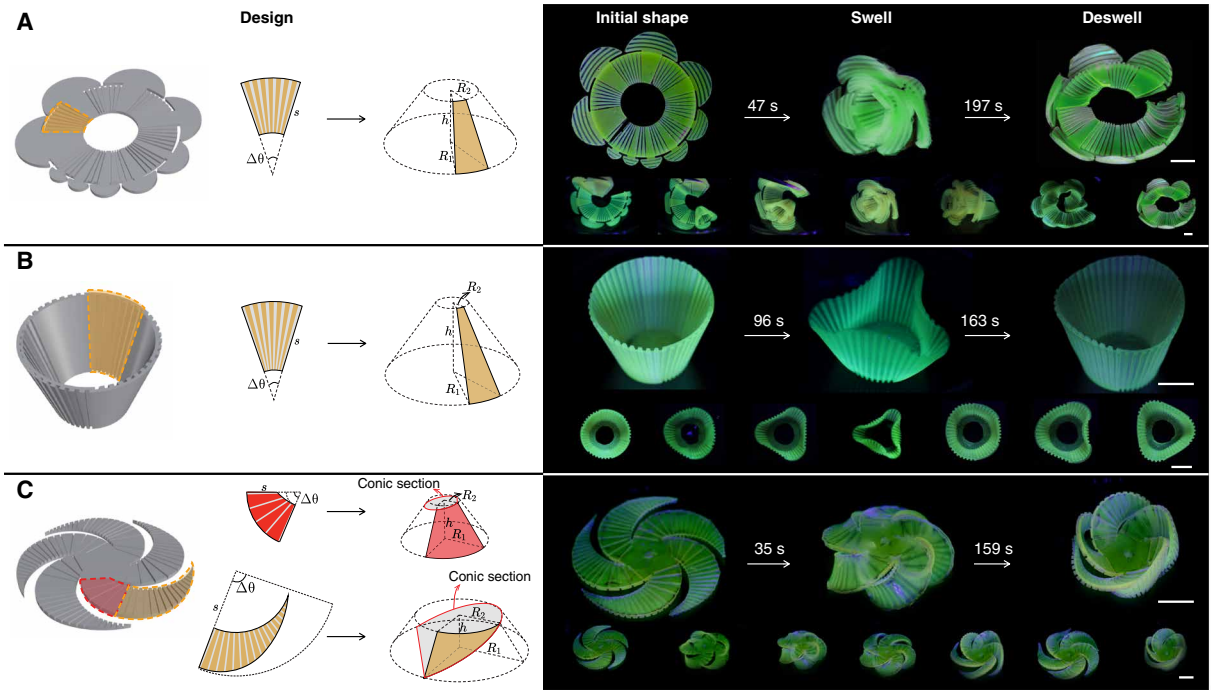

Fig. 5. Design and experiments with extended PDMS sample shapes with zero Gaussian curvatures. (**A**) A rose flower self-folding when swelling and flattening again, with petals bending upwards when deswelling. (**B**) Grooves vertically along the walls of a cup, causing the circular cross section of the cup to morph into a concave polygon when swelling, and a convex polygon when deswelling. (**C**) Initially flat frangipani flower petals bending downward when swelling and upwards when deswelling. Scale bars,10 mm.

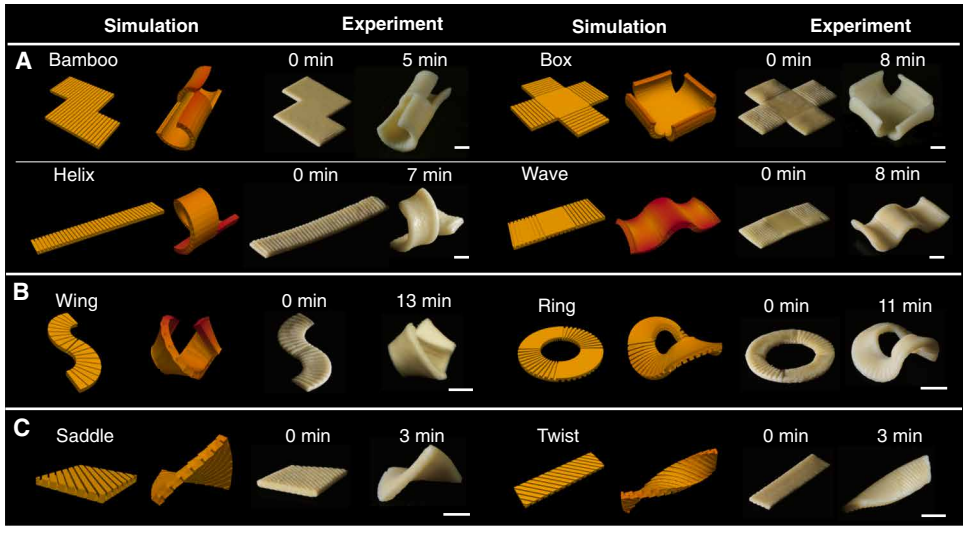

Fig. 6. Design, experiment, and simulation of different morphing pasta shapes before and after cooking. (**A**) Pasta shapes with zero Gaussian curvatures consisting of groups of straight parallel lines. (**B**) Pasta shapes with zero Gaussian curvatures consisting of groups of straight radial lines. (**C**) Pasta shapes with nonzero Gaussian curvatures consisting of straight parallel lines that are on the opposite side of the substrate and overlap one another. Scale bars, 10 mm.

could not be explained by the helical or conical frustum model, they serve as proof of concept for the design of nonzero Gaussian curvature surfaces with double-sided groove and can be explained by analytical work and scaling analysis in the framework of "incompatible elasticity" (*4*, *37*–*39*). Notably, our 3D FE simulations could capture all the pasta shapes very well (Fig. 6 and movie S8), could more accurately guide the morphing design on top of the geometrical model, and could also lay the foundation for systematically exploring the morphing mechanism with more complicated groove patterns.

Applications of morphing food in flat packaging

We used the morphing mechanism to implement a sustainable food packaging method for everyday use, which could save space (59 to 86%, based on volumetric calculations comparing flat shapes with

morphed shapes with regard to the examples shown in Fig. 6) during shipping and storage and partially alleviate pollution by reducing the amount of air shipped during food transportation. For instance, morphing flat pasta into a helical shape when cooked could save up to 60% of the packaging space. An authentic Italian pasta recipe that only requires semolina flour and water was chosen to demonstrate the naturality and simplicity of the concept. We processed all ingredients following the traditional pasta-making process. For highly elastic pasta dough that is hard to extrude or mold, we made thin sheets (2 mm in thickness) using conventional dough-sheeting methods (*40*) and then stamped them using food-graded molds with cuboid-shaped grooves (fig. S1, C to F). A variety of shapes similar to authentic Italian pasta were made (Fig. 6). We followed the conventional pasta cooking process by placing the grooved pasta samples in boiling water. The pasta dough reached its maximum bending curvature within 7 to 12 min, indicating that the pasta was al dente.

DISCUSSION

Asymmetric swelling and deswelling have been leveraged by both natural (*15*, *41*, *42*) and engineered systems (*19*–*24*) for morphing. While most of these systems are composite structures that are anisotropic or inhomogeneous, this work has shown that diffusion-based transient morphing could also be achieved in homogeneous materials with deliberately designed, parametric groove patterns. With parallel and radial groove patterns, flat strips were found to be able to morph into a helix and conical frustum after swelling, respectively. These would serve as the basic building blocks for more complicated, developable 3D shapes, such as flowers. Inspired by shape-morphing in bilayers with orthogonal prestretch or swelling ratios, we further designed double-sided grooves to make nondevelopable 3D surfaces, such as saddles and twists. We believe that this simple yet versatile design process for the fabrication and operation of flat food or flexible soft objects could make morphing materials viable for use with a host of applications, not only enhancing the creativity of scientists from diverse fields but also that of hobbyists, manufacturers, designers, and even chefs. It could have an impact on various real-world contexts, improving the sustainability and efficiency of future manufacturing. In particular, food produced in a flat form could potentially decrease the complexity of machine operations and procedures, saving on manufacturing resources and improving efficiency. The markedly reduced packing space required for shape-changing food could also hopefully reduce food packaging waste.

This work does have certain limitations, and it would be interesting to continue research into groove-based morphing to enable sustainable food design. First, the semianalytical work based on the geometric model cannot fully determine morphing shapes for a helix and conical frustum. It is important to develop a more accurate scaling analysis of these basic building blocks to predict the final shapes of a given material and geometric properties. Second, the current simulation model was based on a nonlinear poroelastic model for ideal polymer networks. However, flour dough is known to be a particularly complicated material, with a mixture of water, starch (composed of amylose and amylopectin), gluten, fiber, and fat, exhibiting highly nonlinear material properties (i.e., viscoplasticity, poroelasticity, and viscoelasticity) (*43*–*46*). Therefore, more accurate simulations need to be developed that include these material nonlinearities and quantify their contributions to food deformation and morphing. Third, the current designs of nondevelopable surfaces were simple and just proofs of concept. Another important future research direction would be the design of general 3D surfaces with more complicated groove patterns, such as double-sided and crossed.

MATERIALS AND METHODS

Chemicals and materials

Morphing pasta samples were fabricated from semolina flour. The PDMS (Sylgard 184) was purchased from Dow Corning Corp. The triggering solvent (diisopropylamine) for the PDMS experiments was purchased from Sigma-Aldrich. The fluorescent dye (Silc Pig™ Electric) used in the PDMS experiments was purchased from Smooth-On Inc. All plastic molds were printed with polylactic acid (PLA) filament, branded as PolyMax PLA from Polymaker Inc.

Fabrication of flour dough samples

For all the pasta experiments introduced in this paper, the sample fabrication process began with dough preparation. This is a semi-manual process that is commonly used in the kitchen. It includes three steps—mixing, sheeting, and cutting (fig. S1). One hundred twelve grams of semolina flour and 43 g of water were poured into a dough mixer (SM-50, Cuisinart) and mixed for 15 to 20 min to produce the dough. The dough was stored in a zipper bag to retain the dough's moisture until the sheeting process. For the sheeting process, a roller sheeter (Atlas 150, Marcato) was used to sheet the dough up to a width of 150 mm, with 10 optional thicknesses from 0.6 to 4.8 mm (defined by the roller nos. 0 to 9). Most of our experimental samples were 2 mm in thickness, which were sheeted sequentially at thickness settings of nos. 0 to 3 once at each setting and then at no. 3 on three more occasions. Last, the dough was cut into the correct size and shape.

The second step was to stamp the pasta with a customized mold, having grooves on one side (fig. S1). The small pitch distances and the sharp tips of the molds are essential for making high-quality (fine and sharp) grooves on the dough; the quality of the grooves will consequently affect the quality of the transformation. To quickly iterate and test the design parameters of the molds, our experiments used 3D-printed molds, printed on an Objet printer (Objet 24, Stratasys Inc.) with a 16-μm printing resolution setting. We used a food-grade mold release (CRC 03311, CRC Industries Inc.) to make our fabricated molds food safe.

The stamping process can be done either manually or using an automated process. The customized mold was manually pressed into the sheeted dough to produce grooves, such that the dough exhibited shape-changing behavior. Since the groove depth tends to vary depending on the applied pressure, stoppers were added to both sides of the mold to maintain groove depth consistency during manual grooving. Alternatively, a digital fabrication process was adapted to control a four-axis robotic gantry system for more precise stamping.

The aforementioned shape-changing mechanisms were applied to both fresh and dried dough, with slight variations in the maximum bending angle and swelling rate. Before hydration, the samples were left in the open air for 20 min to maintain consistent experimental conditions.

Fabrication of PDMS samples

For PDMS-related experiments, the samples were cast in our customized molds made of PLA (PolyMax, Polymaker Inc.) and 3D-printed by a commercial fused deposition modeling 3D printer

(Ultimaker 2+, Ultimaker Inc.). The prints were completed on the "extra fine" setting using the Ultimaker Cura software.

At the start of the casting process, the PDMS base and curing agent were mixed in a 10:1 ratio, using a centrifugal mixer (AR-100 Thinky Mixer, Thinky U.S.A., Inc.). The mixture was then slowly poured into the casting mold, where it was allowed to cure for 12 hours. To better visualize the transformations, 0.05 ml of a fluorescent dye (Silc Pig^{TM} Electric, Smooth-On Inc.) was dispensed into 20 mg of PDMS before mixing.

To fabricate the two-part mold required for the sample shown in Fig. 5B (a frustum with textured inner and outer faces), a set of molds was printed using two types of filament materials (fig. S5F). The outer mold was printed with acrylonitrile butadiene styrene (ABS) and the inner mold with PLA. The glass transition temperatures of ABS and PLA were around 105° and 60°C, respectively. At or above the glass transition temperature, the polymer changed from a glassy, brittle state to a softer, rubbery state (hence the deformation). During the casting, we injected the PDMS from the bottom of the outer mold. After the PDMS was cured, we placed the mold into the hot water at 65°C. The inner mold made of PLA started to deform, and we could easily detach the outer mold, inner mold, and the PDMS sample.

SUPPLEMENTARY MATERIALS

Supplementary material for this article is available at http://advances.sciencemag.org/cgi/content/full/7/19/eabf4098/DC1

REFERENCES AND NOTES

1. U.S. Environmental Protection Agency, (EPA), *Reducing Wasted Food & Packaging: A Guide for Food Services and Restaurants* (2015); https:// epa.gov/sites/production/files/2015-08/documents/reducing_wasted_food_pkg_tool.pdf. [the easiest access to this source is via the URL]
2. W. Wang, L. Yao, T. Zhang, C.-Y. Cheng, D. Levine, H. Ishii, Transformative Appetite: shape-changing food transforms from 2D to 3D by water interaction through cooking, in *Proceedings of the 2017 CHI Conference on Human Factors in Computing Systems* (ACM, New York, NY, USA, 2017), pp. 6123–6132.
3. Y. Tao, Y. Do, H. Yang, Y.-C. Lee, G. Wang, C. Mondoa, J. Cui, W. Wang, L. Yao, Morphlour: personalized flour-based morphing food induced by dehydration or hydration method, in *Proceedings of the 32nd Annual ACM Symposium on User Interface Software and Technology* (ACM, New York, NY, USA, 2019), pp. 329–340.
4. A. Sydney Gladman, E. A. Matsumoto, R. G. Nuzzo, L. Mahadevan, J. A. Lewis, Biomimetic 4D printing. *Nat. Mater.* **15**, 413–418 (2016).
5. Y. Kim, H. Yuk, R. Zhao, S. A. Chester, X. Zhao, Printing ferromagnetic domains for untethered fast-transforming soft materials. *Nature* **558**, 274–279 (2018).
6. R. M. Erb, J. S. Sander, R. Grisch, A. R. Studart, Self-shaping composites with programmable bioinspired microstructures. *Nat. Commun.* **4**, 1712 (2013).
7. T. van Manen, S. Janbaz, A. A. Zadpoor, Programming 2D/3D shape-shifting with hobbyist 3D printers. *Mater. Horiz.* **4**, 1064–1069 (2017).
8. H. Thérien-Aubin, Z. L. Wu, Z. Nie, E. Kumacheva, Multiple shape transformations of composite hydrogel sheets. *J. Am. Chem. Soc.* **135**, 4834–4839 (2013).
9. J. Kim, J. A. Hanna, M. Byun, C. D. Santangelo, R. C. Hayward, Designing responsive buckled surfaces by halftone gel lithography. *Science* **335**, 1201–1205 (2012).
10. J. Wu, Z. Zhao, X. Kuang, C. M. Hamel, D. Fang, H. J. Qi, Reversible shape change structures by grayscale pattern 4D printing. *Multifunct. Mater.* **1**, 015002 (2018).
11. L. Huang, R. Jiang, J. Wu, J. Song, H. Bai, B. Li, Q. Zhao, T. Xie, Ultrafast digital printing toward 4D shape changing materials. *Adv. Mater.* **29**, 1605390 (2017).
12. Y. Klein, E. Efrati, E. Sharon, Shaping of elastic sheets by prescription of non-Euclidean metrics. *Science* **315**, 1116–1120 (2007).
13. Q. Ge, C. K. Dunn, H. J. Qi, M. L. Dunn, Active origami by 4D printing. *Smart Mater. Struct.* **23**, 094007 (2014).
14. A. Cangialosi, C. K. Yoon, J. Liu, Q. Huang, J. Guo, T. D. Nguyen, D. H. Gracias, R. Schulman, DNA sequence–directed shape change of photopatterned hydrogels via high-degree swelling. *Science* **357**, 1126–1130 (2017).
15. E. Reyssat, L. Mahadevan, Hygromorphs: From pine cones to biomimetic bilayers. *J. R. Soc. Interface* **6**, 951–957 (2009).
16. M. M. Hamedi, V. E. Campbell, P. Rothemund, F. Güder, D. C. Christodouleas, J.-F. Bloch, G. M. Whitesides, Electrically activated paper actuators. *Adv. Funct. Mater.* **26**, 2446–2453 (2016).
17. Y. Liu, J. K. Boyles, J. Genzer, M. D. Dickey, Self-folding of polymer sheets using local light absorption. *Soft Matter* **8**, 1764–1769 (2012).
18. Z. L. Wu, M. Moshe, J. Greener, H. Therien-Aubin, Z. Nie, E. Sharon, E. Kumacheva, Three-dimensional shape transformations of hydrogel sheets induced by small-scale modulation of internal stresses. *Nat. Commun.* **4**, 1586 (2013).
19. J. Odent, S. Vanderstappen, A. Toncheva, E. Pichon, T. J. Wallin, K. Wang, R. F. Shepherd, P. Dubois, J.-M. Raquez, Hierarchical chemomechanical encoding of multi-responsive hydrogel actuators via 3D printing. *J. Mater. Chem. A* **7**, 15395–15403 (2019).
20. Z. Ji, C. Yan, B. Yu, X. Zhang, M. Cai, X. Jia, X. Wang, F. Zhou, 3d printing of hydrogel architectures with complex and controllable shape deformation. *Adv. Mater. Technol.* **4**, 1800713 (2019).
21. A. Lucantonio, P. Nardinocchi, L. Teresi, Transient analysis of swelling-induced large deformations in polymer gels. *J. Mech. Phys. Solids* **61**, 205–218 (2013).
22. M. Curatolo, P. Nardinocchi, E. Puntel, L. Teresi, Transient instabilities in the swelling dynamics of a hydrogel sphere. *J. Appl. Phys.* **122**, 145109 (2017).
23. H. Lee, J. Zhang, H. Jiang, N. X. Fang, Prescribed pattern transformation in swelling gel tubes by elastic instability. *Phys. Rev. Lett.* **108**, 214304 (2012).
24. Q. Li, Z. Xu, S. Ji, P. Lv, X. Li, W. Hong, H. Duan, Kinetics-induced morphing of three-dimensional-printed gel structures based on geometric asymmetry. *J. Appl. Mech.* **87**, 071008 (2020).
25. H.-B. Liu, H.-Q. Gong, Templateless prototyping of polydimethylsiloxane microfluidic structures using a pulsed CO_2 laser. *J. Micromech. Microeng.* **19**, 037002 (2009).
26. Y. Cao, R. Mezzenga, Design principles of food gels. *Nat. Food.* **1**, 106–118 (2020).
27. J. N. Lee, C. Park, G. M. Whitesides, Solvent compatibility of poly(dimethylsiloxane)-based microfluidic devices. *Anal. Chem.* **75**, 6544–6554 (2003).
28. Y. Hu, X. Chen, G. M. Whitesides, J. J. Vlassak, Z. Suo, Indentation of polydimethylsiloxane submerged in organic solvents. *J. Mater. Res.* **26**, 785–795 (2011).
29. D. P. Holmes, M. Roché, T. Sinha, H. A. Stone, Bending and twisting of soft materials by non-homogenous swelling. *Soft Matter* **7**, 5188–5193 (2011).
30. Y. Mao, L. Anand, A theory for fracture of polymeric gels. *J. Mech. Phys. Solids* **115**, 30–53 (2018).
31. S. A. Chester, C. V. Di Leo, L. Anand, A finite element implementation of a coupled diffusion-deformation theory for elastomeric gels. *Int. J. Solids Struct.* **52**, 1–18 (2015).
32. J. E. Dexter, R. R. Matsuo, B. C. Morgan, Spaghetti stickiness: Some factors influencing stickiness and relationship to other cooking quality characteristics. *J. Food Sci.* **48**, 1545–1551 (1983).
33. S. Nakamura, H. Satoh, K. Ohtsubo, Development of formulae for estimating amylose content, amylopectin chain length distribution, and resistant starch content based on the iodine absorption curve of rice starch. *Biosci. Biotechnol. Biochem.* **79**, 443–455 (2015).
34. H. M. Elmehdi, M. G. Scanlon, J. H. Page, M. I. P. Kovacs, Probing thermal transitions and structural properties of gluten proteins using ultrasound. *J. Ultrasound* **16**, 101–110 (2013).
35. M. Schirmer, M. Jekle, T. Becker, Starch gelatinization and its complexity for analysis. *Starch - Stärke.* **67**, 30–41 (2015).
36. Q. Zhang, J. Wommer, C. O'Rourke, J. Teitelman, Y. Tang, J. Robison, G. Lin, J. Yin, Origami and kirigami inspired self-folding for programming three-dimensional shape shifting of polymer sheets with light. *Extreme Mech. Lett.* **11**, 111–120 (2017).
37. Z. Chen, Q. Guo, C. Majidi, W. Chen, D. J. Srolovitz, M. P. Haataja, Nonlinear geometric effects in mechanical bistable morphing structures. *Phys. Rev. Lett.* **109**, 114302 (2012).
38. W. M. van Rees, E. Vouga, L. Mahadevan, Growth patterns for shape-shifting elastic bilayers. *Proc. Natl. Acad. Sci. U.S.A.* **114**, 11597–11602 (2017).
39. S. Armon, E. Efrati, R. Kupferman, E. Sharon, Geometry and mechanics in the opening of chiral seed pods. *Science* **333**, 1726–1730 (2011).
40. L. Levine, B. A. Drew, Rheological and Engineering Aspects of the Sheeting and Laminating of Doughs, in *Dough Rheology and Baked Product Texture*, H. Faridi, J. M. Faubion, Eds. (Springer, 1990), pp. 513–555.
41. R. Elbaum, L. Zaltzman, I. Burgert, P. Fratzl, The role of wheat awns in the seed dispersal unit. *Science* **316**, 884–886 (2007).
42. N. E. Stamp, Self-burial behaviour of erodium cicutarium seeds. *J. Ecol.* **72**, 611–620 (1984).
43. S. Sahin, S. G. Sumnu, Rheological properties of foods, in *Physical Properties of Food* (Springer, 2006), pp. 39–105.
44. B. J. Dobraszczyk, M. P. Morgenstern, Rheology and the breadmaking process. *J. Cereal Sci.* **38**, 229–245 (2003).
45. J. M. Faubion, R. C. Hoseney, The viscoelastic properties of wheat flour doughs, in *Dough Rheology and Baked Product Texture*, H. Faridi, J. M. Faubion, Eds. (Springer, 1990), pp. 29–66.

46. H. Zhu, A. Dhall, S. Mukherjee, A. K. Datta, A model for flow and deformation in unsaturated swelling porous media. *Transp. Porous Media.* **84**, 335–369 (2010).
47. A. Dorfmann, R. W. Ogden, Nonlinear electroelastic deformations. *J. Elast.* **82**, 99–127 (2006).
48. A. Logg, K.-A. Mardal, G. Wells, *Automated Solution of Differential Equations by the Finite Element Method: the FEniCS Book* (Springer, ed. 1, 2012), vol. 84.
49. R. G. M. van der Sman, M. B. J. Meinders, Prediction of the state diagram of starchwater mixtures using the Flory–Huggins free volume theory. *Soft Matter* **7**, 429–442 (2011).

Acknowledgments: We thank C. Wei, J. Forman, and J. Gu for insightful suggestions. **Funding**: This project acknowledges funding support from the U.S. National Science Foundation (IIS-2017008 and CMMI-CAREER-1847149), the Carnegie Mellon University Manufacturing Futures Initiative that was made possible by the Richard King Mellon Foundation, and the National Natural Science Foundation of China (61672451 and 62002321). Simulations were performed at the Triton Shared Computing Cluster at the San Diego Supercomputer Center and the Comet cluster (award TG-MSS170004 to T.Z.) in The Extreme Science and Engineering Discovery Environment. **Author contributions**: Y.T., Y.-C.L., J.S., J.C., C.M., L.S., and G.W. conducted the pasta and PDMS experiments. Y.D. and H.Y. developed the digital stamping process. X.Z., D.Li., and M.B. conducted the FE analysis. H.L. and Y.-C.L. conducted the compression test of the pasta disks. D.Lu. captured the SEM images. W.W., T.Z., and L.Y. supervised the research. All authors contributed to the manuscript writing. **Competing interests**: There is a patent related to this work filed by Carnegie Mellon University and Syracuse University with the U.S. patent office (assignors: L.Y., W.W., Y.T., Y.-C.L., H.L., J.C., C.M., J.S., and T.Z.; international application no. PCT/US2020/039023; filing date: 22 June 2020; publication date: 24 December 2020). The other authors declare that they have no competing interests. **Data and materials availability**: All data needed to evaluate the conclusions in the paper are present in the paper and/or the Supplementary Materials. Additional data related to this paper may be requested from the authors.

Submitted 29 November 2020
Accepted 16 March 2021
Published 5 May 2021
10.1126/sciadv.abf4098

Citation: Y. Tao, Y.-C. Lee, H. Liu, X. Zhang, J. Cui, C. Mondoa, M. Babaei, J. Santillan, G. Wang, D. Luo, D. Liu, H. Yang, Y. Do, L. Sun, W. Wang, T. Zhang, L. Yao, Morphing pasta and beyond. *Sci. Adv.* **7**, eabf4098 (2021).

Science Advances

Morphing pasta and beyond

Ye Tao, Yi-Chin Lee, Haolin Liu, Xiaoxiao Zhang, Jianxun Cui, Catherine Mondoa, Mahnoush Babaei, Jasio Santillan, Guanyun Wang, Danli Luo, Di Liu, Humphrey Yang, Youngwook Do, Lingyun Sun, Wen Wang, Teng Zhang and Lining Yao

Sci Adv **7** (19), eabf4098.
DOI: 10.1126/sciadv.abf4098

Science Advances (ISSN 2375-2548) is published by the American Association for the Advancement of Science, 1200 New York Avenue NW, Washington, DC 20005. The title *Science Advances* is a registered trademark of AAAS.

Science Advances
AAAS

advances.sciencemag.org/cgi/content/full/7/19/eabf4098/DC1

Supplementary Materials for

Morphing pasta and beyond

Ye Tao, Yi-Chin Lee, Haolin Liu, Xiaoxiao Zhang, Jianxun Cui, Catherine Mondoa, Mahnoush Babaei, Jasio Santillan, Guanyun Wang, Danli Luo, Di Liu, Humphrey Yang, Youngwook Do, Lingyun Sun, Wen Wang*, Teng Zhang*, Lining Yao*

*Corresponding author. Email: wen.wang@rd.nestle.com (W.W.); tzhang48@syr.edu (T.Z.); liningy@andrew.cmu.edu (L.Y.)

Published 5 May 2021, *Sci. Adv.* **7**, eabf4098 (2021)
DOI: 10.1126/sciadv.abf4098

The PDF file includes:

Other Supplementary Material for this manuscript includes the following:

(available at advances.sciencemag.org/cgi/content/full/7/19/eabf4098/DC1)

Supplementary Text

Triggering setup and conditions

Quantitative pasta testing was conducted using a glass container equipped with an infusion heater. The water was brought up to 90 °C before adding the pasta. The water was then kept between 85 and 90 °C with intermittent heating to prevent boiling, which can affect the transformation. Shortly after adding the pasta to the hot water, it began to transform, reaching its maximum bending angle after around 12 minutes, and retaining this angle for around 20 minutes before beginning to bend back. As the material began to bend in the opposite direction, some disintegration was observed.

For the PDMS samples, diisopropylamine was used as a triggering agent. Upon submerging, the PDMS sample immediately began to swell, reaching its maximum bending angle after around six minutes. Since diisopropylamine evaporates rapidly in air, the de-swelling began as soon as the PDMS sample was removed, bending back to a flat state after around two to three minutes. The sample then continued to bend in the opposite direction to a maximum bending angle after around one to two minutes, before decreasing again and de-swelling to its initial shape and size a few hours later.

Measurement method for strip-based swelling tests

For the strip bending angle measurements for both the pasta and the PDMS in Fig 1, fig S2 and S3, we took side-view photographs of the samples. These images were outlined with a computer-aided design tool (i.e., Rhinoceros 3D) using Bezier curves. The angle between the tangential vectors at both ends of the pasta outlines was measured. The maximum bending angle deviation measured was less than 10% in our repeatability tests. The bending curvature was calculated by dividing the bending angle by the strip's length.

To calculate the swelling ratios of the pasta and the PDMS disks in Fig. 2, top-view photographs were taken during swelling, and the changing diameter was measured with ImageJ software.

Compression test

To characterize the mechanical properties of the dough after different levels of hydration, uniaxial compression tests (fig. S7) with a compression rate of 0.005 mm/s and a maximum strain of 0.20 were conducted. The pasta dough was prepared in disks with an initial diameter of 18.94 mm and boiled in water for different amounts of time. These thicknesses and the diameters of the various samples are shown in table S2. The compression stress was calculated by dividing the compression force by the initial area of each pasta sample, representing the engineering stress.

Characterization of the initial elastic modulus

During the compression test (three to four minutes), the water diffusion in the pasta was neglected so that it could be approximately modeled as a hyperelastic material. In this work, the incompressible Neo-Hookean stress-strain formulation was chosen to describe the material's elastic behaviors. Since the pasta's stress-strain curves were obtained through a series of uniaxial compression experiments, the relationship between the material's engineering stress and stretch can be represented as (*47*):

$$\sigma_{11}^{\mathrm{eng}} = 2C_1\left(\lambda - \frac{1}{\lambda^2}\right), \tag{1}$$

where σ_{11} denotes the engineering stress, λ denotes the stretch ratio ($\lambda<1$ for our compression tests) and C_1 is a material constant. According to the Neo-Hookean formulation, $2C_1$ represents the material's shear modulus and $6C_1$ represents the material's Young's modulus by assuming the material's incompressibility.

During the uniaxial compression experiments, seven different pasta samples cooked for different durations were tested (shown in table S2). We conducted separate fitting for all pasta samples and calculated the corresponding material parameters based on the fitted C_1. For each sample, the fitting was conducted using the data from the first 8% strain (strain range: 0 ~ -0.08), and the corresponding material parameters were calculated based on the fitted C1. All the fitting parameters and corresponding calculated material parameters are shown in table S2.

The fitted result of the uncooked pasta sample (cooking time = 0 minutes) (fig. S7), where $C_1 = 0.0223$ MPa was used to calculate the modulus of the model. The curve follows the Neo-Hookean formulation, representing the material's hyperelastic behavior. Assuming the material is elastic and incompressible (Poisson's ratio $v = 0.5$), we have shear modulus $G = 2C_1$ (C_1 is the fitting parameter) and Young's Modulus $E = 2G(1+v) = 6C_1$.

Modeling and simulation

To establish the design for our morphing food using grooved surface microstructures, we adopted a coupled diffusion and deformation model for the polymeric gels to simulate the dynamic morphing of pasta during cooking. Here, we only review the key equations of the theoretical model and refer readers to the original papers (*30*, *31*) for more details. The basic fields related to this theory can be found in table S3.

The governing equations of the polymeric gels include the balance of forces and the balance of fluid concentration. For the balance of forces, the governing equations are

$$\mathrm{div}\boldsymbol{T} = \boldsymbol{0}, \tag{2}$$

with the Cauchy stress $\boldsymbol{T}$ is given by

$$\boldsymbol{T} = J^{-1}[G(\boldsymbol{B} - \boldsymbol{I}) + K(\ln J^e)\boldsymbol{I}], \tag{3}$$

where G and K are shear and bulk modulus, respectively. Here the body forces are neglected.

For the balance of fluid concentration, the governing equation is

$$\dot{c_R} = -J\mathrm{div}\boldsymbol{j}, \tag{4}$$

with $\boldsymbol{j} = -m\mathrm{grad}\mu$ and the chemical potential given by

$$\mu = \mu^0 + R\vartheta(\ln(1-\phi) + \phi + \chi\phi^2) - J^{s^{-1}}\Omega K(\ln J^e), \tag{5}$$

where R is the gas constant, ϑ is the temperature, χ is the Flory–Huggins interaction parameter, and $m = Dc/(R\vartheta)$ with D representing a diffusion coefficient.

Since the structures can freely deform in our experiments, we did not assign displacement boundary conditions in the simulations. The swelling and de-swelling processes were modeled by prescribing a time-dependent chemical potential on the outer surfaces of the structures,

$$\breve{\mu} = \mu^0 + \mu_0 \exp(-t/t_d), \tag{6}$$

where t_d is a characteristic time scale associated with the structure surface interaction with the environment, and treated as a fitting parameter in the current work to match the morphing of the structures. From numerical tests, we found that the steep change in the chemical potential in the de-swelling process will cause convergence issues with regard to the simulations. To overcome this, we smoothed the chemical potential change near the starting point of the de-swelling with the Fermi-Dirac function.

The governing equations in Eqs. (2-6) were solved by the finite element method through a user-defined element (UEL) in ABAQUS/standard (*31*). From our numerical tests, we found that the UEL works very well with relatively stiff materials, like PDMS, and can also capture the structure collision. However, we encountered numerical convergence issues for very soft materials, like pasta. Therefore, we further implemented the finite element schemes in FEniCS (*48*) to solve the governing equations. Although the FEniCS can resolve the numerical convergence issues for very soft materials, it cannot handle the structure collision. Therefore, both ABAQUS and FEniCS were needed to capture the morphing with and without contact. More specifically, the PMDS structures in Figs. 1 and 2 were simulated with ABAQUS. The PDMS structures in Figs. 3 and 4 and all the pasta simulations were carried out with FEniCS. For the pasta simulations in Fig. 6, the simulation meshes were generated by importing the CAD files used in creating grooved structures in the experiments into a mesh generation software (ABAQUS and Gmsh).

By fitting the compression and the swelling of the pasta disks, and the swelling of the PDMS disks, we obtained the key material properties of the pasta and the PDMS, as shown in table S1. The Flory–Huggins interaction parameter, χ, was taken from the literature (*31*, *49*). It should be noted that χ for pasta was known to be dependent on water concentration. Here, we chose a typical value ($\chi = 0.5$) representing the swelling process of pasta. Future studies are needed to develop more sophisticated models to capture the nonlinear changes of χ. To normalize the disk swelling data in Fig. 2A, we divided the time by its diffusion characteristic time scale,τ, given by

$$\tau = H^2/D, \tag{7}$$

where H is the thickness of the disk and D is the diffusion coefficient. For the pasta ($H = 2$ mm) and the PDMS ($H = 0.9$ mm) disks, the calculated diffusion characteristic time scales were $\tau_{\text{pasta}} = 2000\ s$ and $\tau_{\text{PDMS}} = 405\ s$.

Supplementary Materials

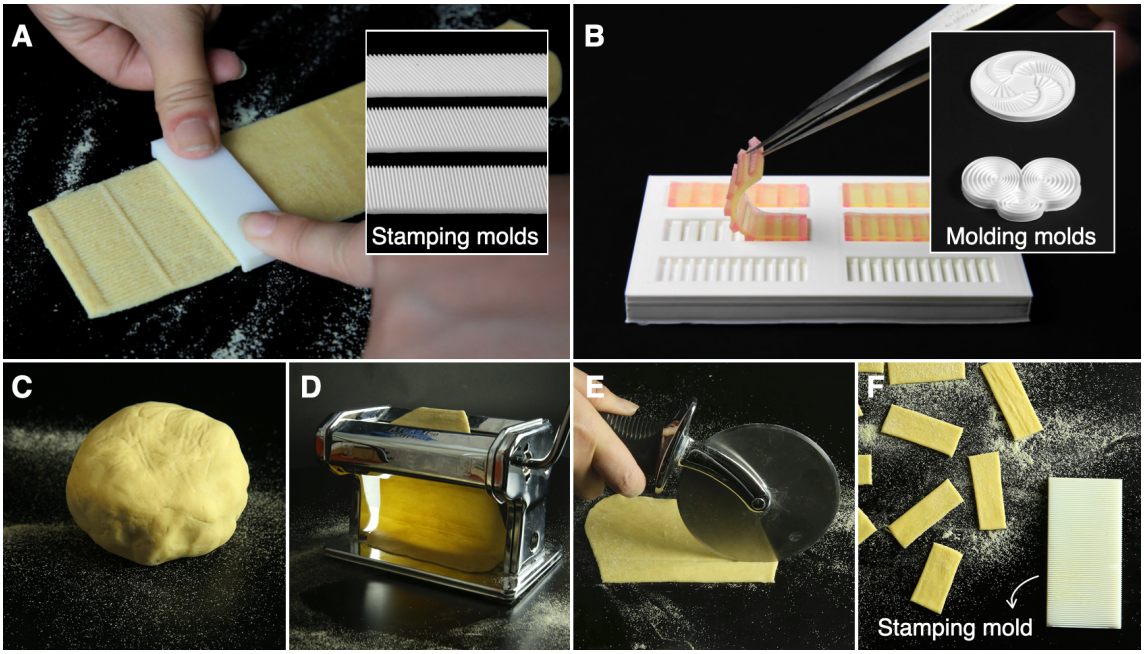

Fig. S1. Fabrication process of the grooved samples. (**A**) Stamping to create grooved samples with pasta dough. (**B**) Molding and casting to create grooved samples with PDMS. (**C** to **F**) The detailed process of creating grooved pasta samples that involves (C) dough mixing, (D) sheeting, (E) cutting and (F) stamping. (Photo Credit: Ye Tao, Carnegie Mellon University)

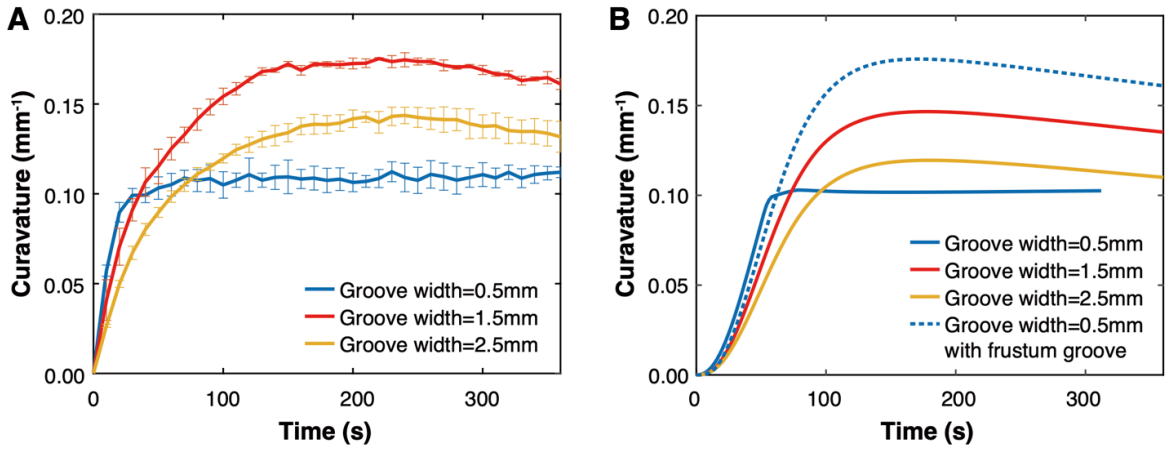

Fig. S2. Comparison of bending in PDMS strips of different groove widths. These strip samples (25.5 mm in length, 5 mm in width, 2 mm in thickness, 1.5 mm in groove gap) were prepared via a molding and casting process, and triggered with diisopropylamine for their dynamic swelling tests. (**A**) The experimental result of three strip samples with cuboidal grooves. This shows that the maximum bending angle increases as the groove width decreases. However, the colliding of the grooves (in the case of groove width = 0.5 mm) can prevent the strip from bending further. (**B**) The simulation result of three strips with cuboidal grooves, and one strip with frustum grooves to minimize the groove collision during bending. The simulation matches well with the general trend of the experiment – disregarding the effects of groove collision, the maximum bending angle increases as the groove width decreases.

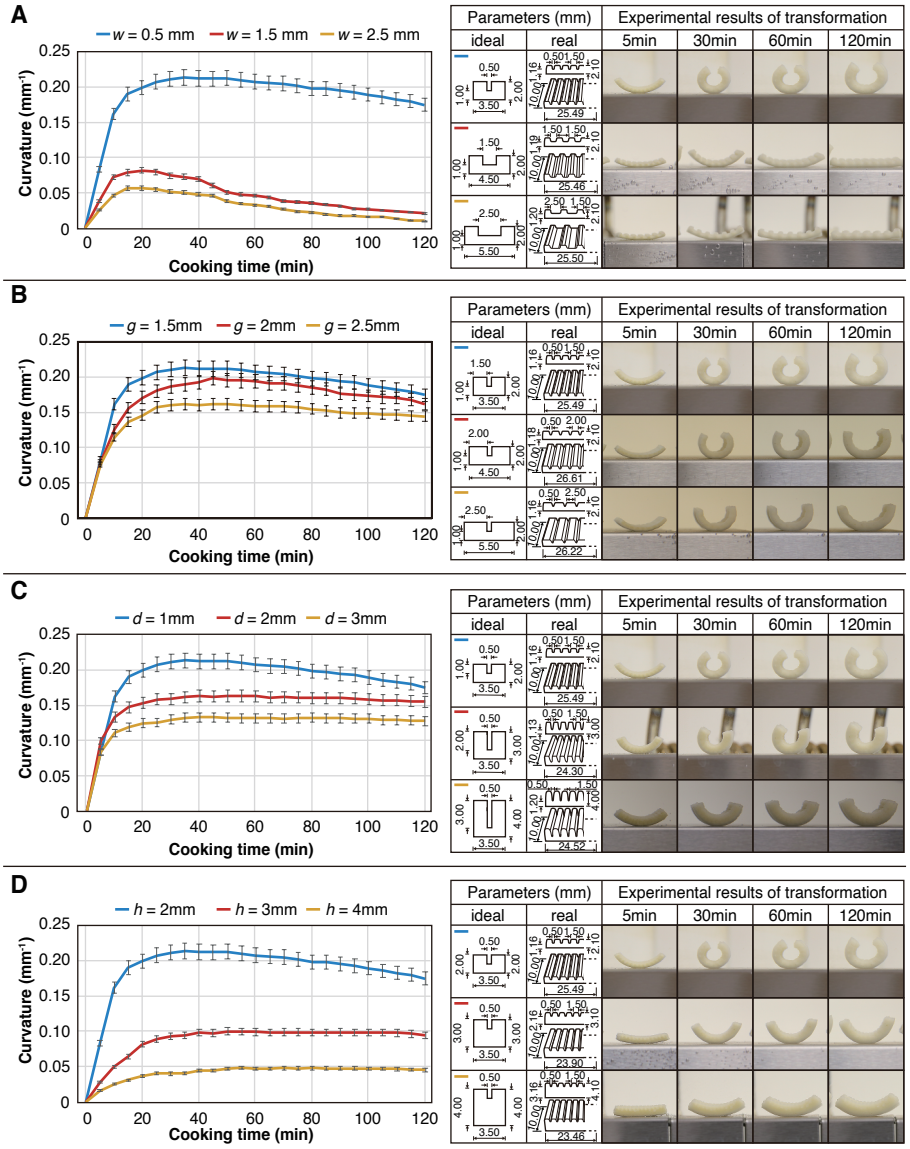

Fig. S3. Experimental results on the geometrical factors of morphing pasta. Pasta strips have different bending performances with varied (**A**) groove width (w), (**B**) groove gap (g), (**C**) groove depth (d) and (**D**) total height (h). (Photo Credit: Ye Tao, Carnegie Mellon University)

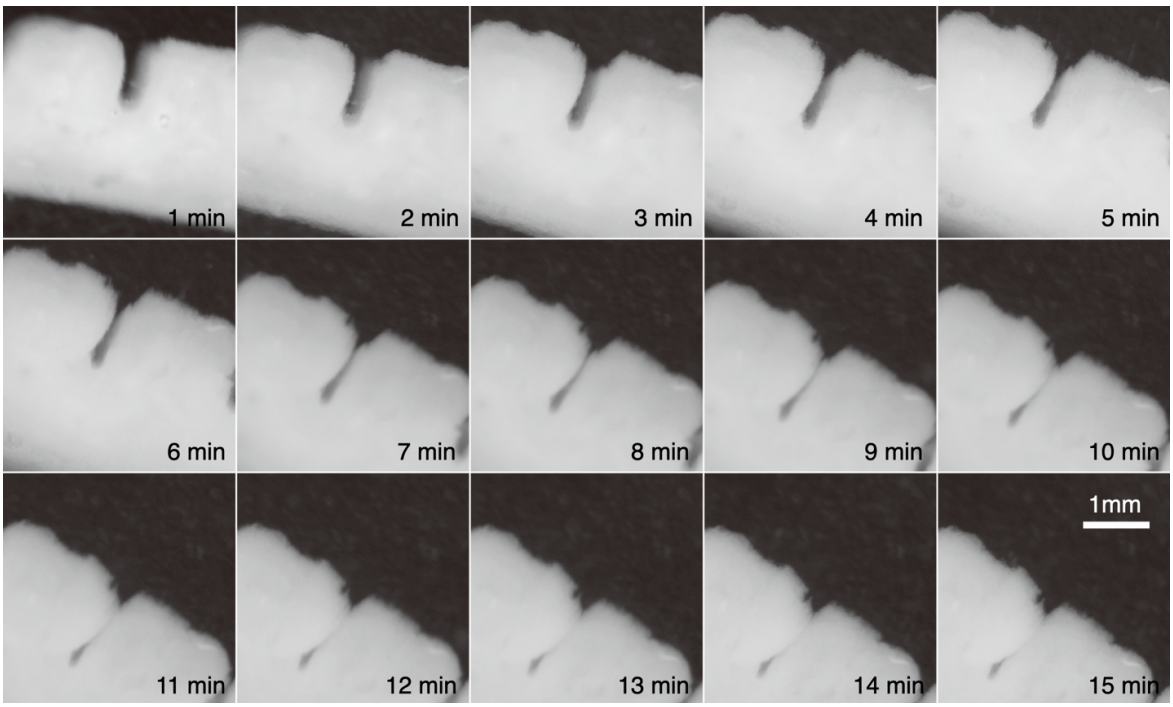

Fig. S4. Microscope images showing pasta groove gaps decreasing over time as the strip swells and changes shape. The gaps continue to narrow until neighboring grooves collide and push against each other.

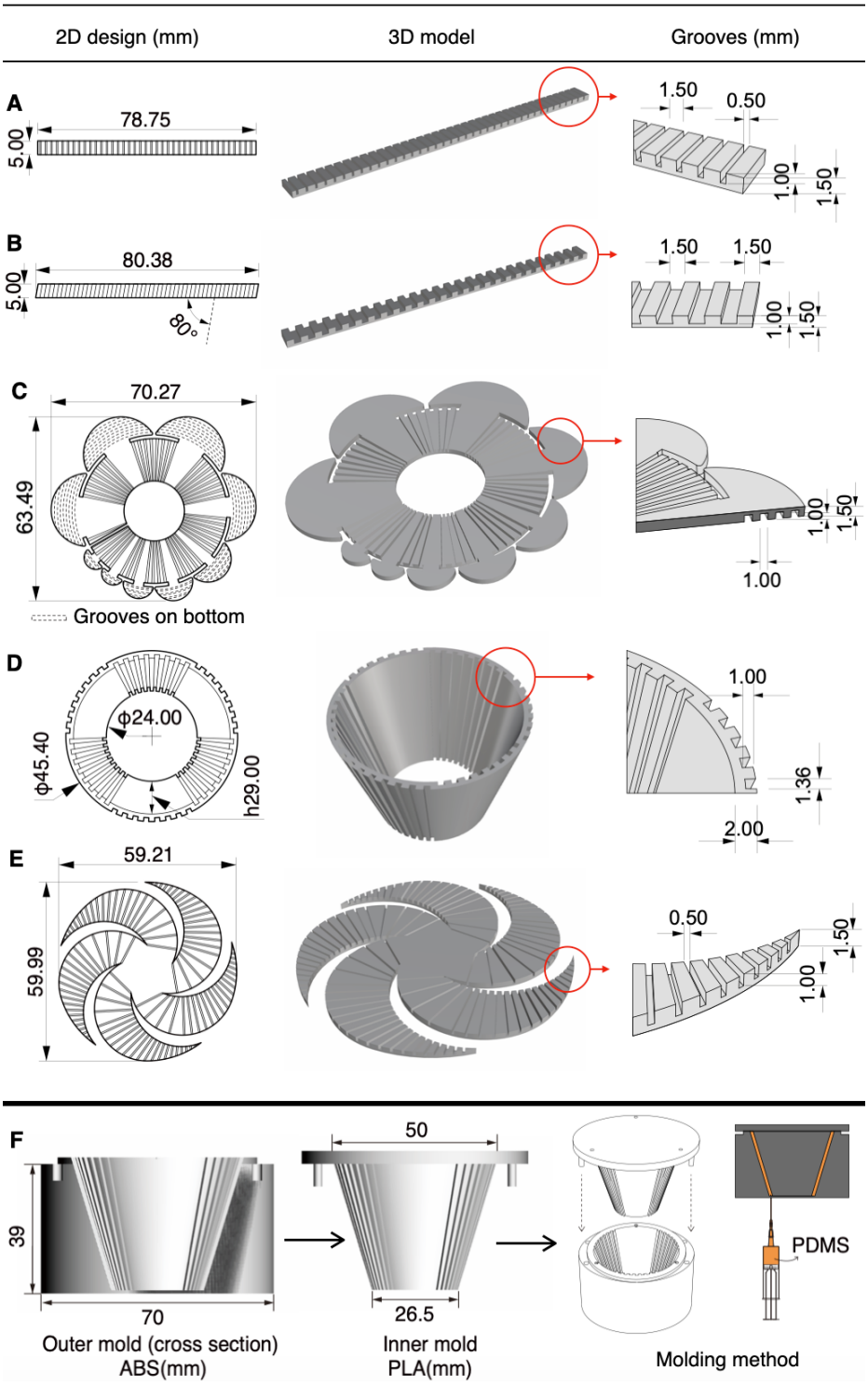

Fig. S5. Geometrical features of morphing PDMS samples, shown in Figs. 3 and 5. For each sample, a 2D design schematic, a 3D model and detailed groove dimensions are shown.

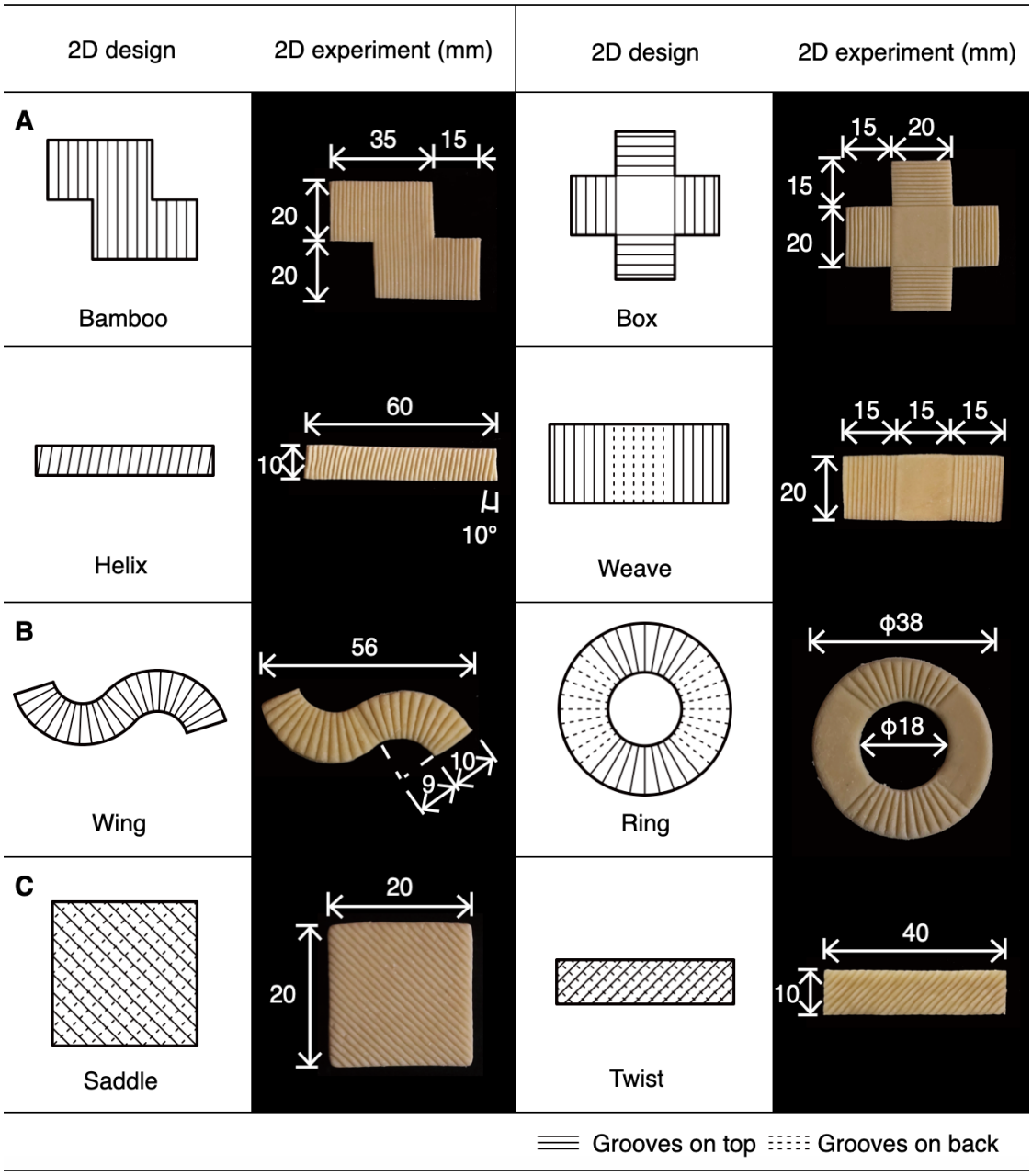

Fig. S6. Various morphing pasta samples fabricated in Fig. 6. In each case, a design schematic and a photograph of the flat sample are shown. The thickness of all the samples is 2 mm. (Photo Credit: Ye Tao, Carnegie Mellon University)

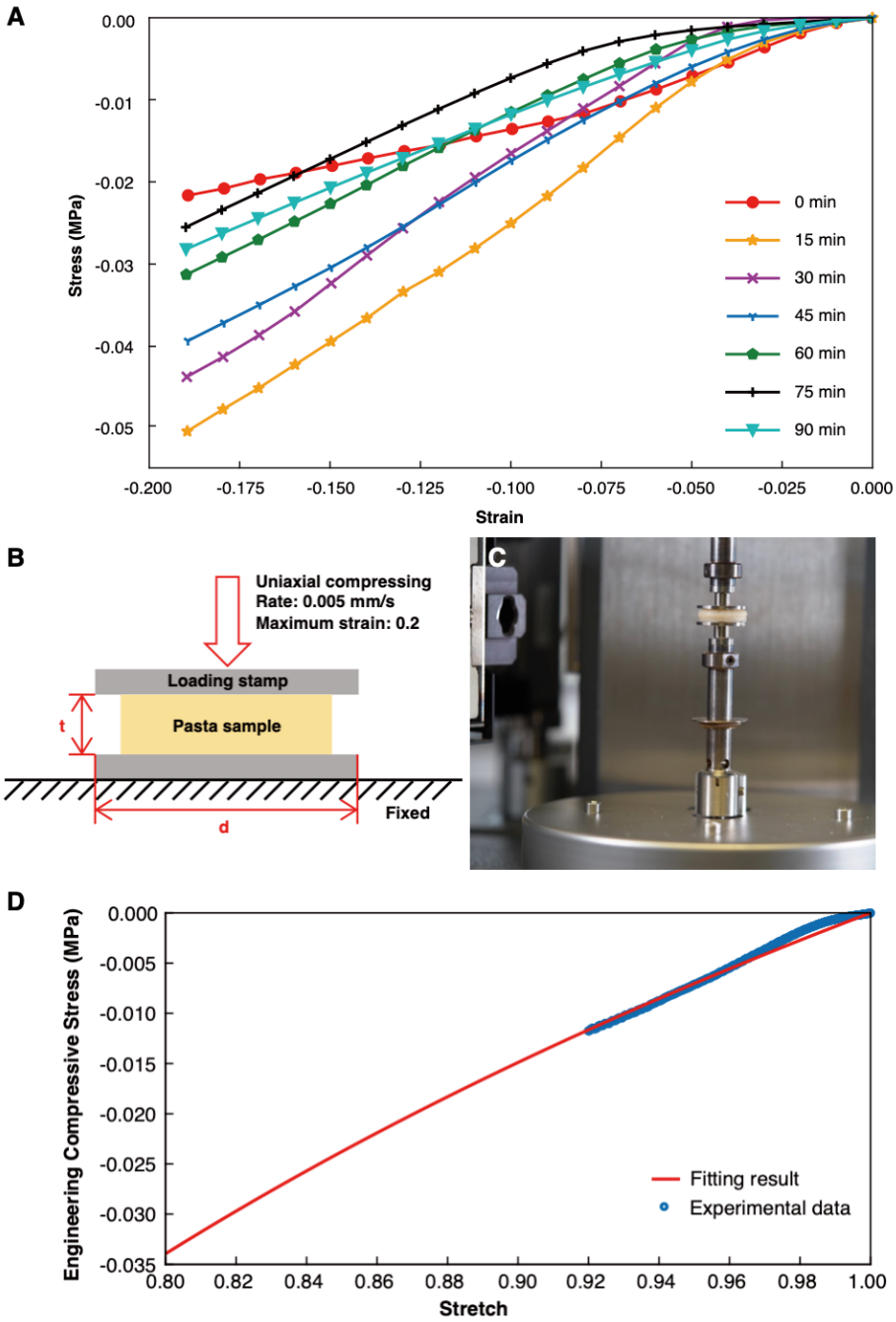

Fig. S7. Uniaxial compression tests of disk-shaped pasta specimens. (**A**) Test results. (**B** to **C**) Diagram and photograph of the testing setup of disk-shaped pasta specimens, where the gray blocks represent the loading stamp and the yellow block represents the compressed pasta sample. *t* and *d* denote the thickness and the diameter of the pasta sample, respectively. The specimens have the same initial diameter of 18.94 mm and were cooked in water at 90 °C for different time durations before each test. A compression rate of 0.005 mm/s and a maximum strain of 0.20 were used to identify the dough's elastic response under different hydration conditions. (**D**) The fitting result of the pasta sample before cooking (cooking time = 0 min), where the fitting parameter $C_1 = 0.0223$ MPa. The curve following the Neo-Hookean formulation represents the material's hyperelastic behavior. (Photo Credit: Lining Yao, Carnegie Mellon University)

	χ	D (m^2/s)	ϕ_0	Ω (m^3/mol)	G (Mpa)	K (MPa)	t_d (s)
PDMS	0.1	2.0e-9	0.99	1.e-4	1	100	16
Pasta	0.5	2.0e-9	0.9	1.e-4	0.045	4.5	60

Table S1. Fitting parameters of PDMS and pasta.

Samples	Cooking Time / min	Initial Thickness / mm	Diameter / mm	Fitting Parameter (C_1)	Shear Modulus (G) / MPa	Young's Modulus (E) / MPa
1	0	5.5	18.94	0.0223	0.0445	0.1335
2	15	5.7	20.21	0.0285	0.0571	0.1713
3	30	5.4	21.12	0.0141	0.0283	0.0849
4	45	6.1	21.95	0.0207	0.0414	0.1243
5	60	6.3	22.64	0.0106	0.0212	0.0636
6	75	6.2	22.75	0.0058	0.0117	0.0350
7	90	6.2	23.02	0.0138	0.0277	0.0830

Table S2. The geometrical parameters, fitting results and calculated material parameters of pasta disks after varying cooking times. Assuming the material is elastic and incompressible (Poisson's ratio $\nu = 0.5$), we have shear modulus $G = 2C_1$ (C_1 is the fitting parameter) and Young's Modulus $E = 2\,G(1+\nu) = 6C_1$.

c_R	fluid concentration in the undeformed body
c_{R0}	Initial fluid concentration in the undeformed body
$c = J^{-1}c_R$	fluid concentration in the deformed body
Ω	volume of a mole of fluid molecules
$\lambda^s = (1 + \Omega(c_R - c_{R0}))^{1/3}$	Swelling stretch
$\phi = \frac{1 - \Omega c_{R0}}{1 + \Omega(c_R - c_{R0})}$	polymer volume fraction
$\phi_0 = 1 - \Omega c_{R0}$	Initial polymer volume fraction
μ	chemical potential
μ^0	a reference chemical potential for the fluid
m	mobility
$\boldsymbol{j}$	spatial flux
$\boldsymbol{F},\ J = det\boldsymbol{F}$	deformation gradient
$\boldsymbol{F} = \boldsymbol{F}^e\boldsymbol{F}^s$	multiplicative decomposition of $\boldsymbol{F}$
$\boldsymbol{F}^e, J^e = det\boldsymbol{F}^e$	elastic part of the deformation gradient $\boldsymbol{F}$
$\boldsymbol{F}^s = \lambda^s\boldsymbol{I}$	swelling part of the deformation gradient $\boldsymbol{F}$
$\boldsymbol{B} = \boldsymbol{F}\boldsymbol{F}^T$	left Cauchy–Green tensor based on $\boldsymbol{F}$
$\boldsymbol{T}$	Cauchy stress tensor

Table S3. Parameters and variables in the polymeric gel model.

Description of supplementary videos

Movie S1. Straight-line pasta morphs into a helix (8x actual speed). Demonstrates a home-cooking scenario where the triggering condition is food-safe. The line pasta is 200 mm in length, 2 mm in width and 2 mm in thickness. The initial dimensions of the Frustum shaped grooves are 1.5 mm in the gaps, 0.5 mm in width and 1.8 mm in depth.

Movie S2. Simulation and experiment of a bi-directional PDMS strip. This shows that the strip exhibits dynamic, bi-directional bending behavior as it swells in diisopropylamine and de-swells in air. The strip sample is 25.5 mm in length, 5 mm in width, 2 mm in thickness, 1.5 mm in both groove gaps and width, and 1 mm in groove depth.

Movie S3. Microscopic view of the morphing of pasta grooves during the cooking process (50x actual speed). The neighboring grooves collide and push against each other as the pasta strip swells. The initial dimensions of the grooves are 1.5 mm in the gaps, 0.5 mm in width and 1 mm in depth.

Movie S4. Bi-directional and reversible morphing of 2D and 3D coils made of PDMS. The swelling is triggered in diisopropylamine and the de swelling occurs in the open air.

Movie S5. Bi-directional and reversible morphing of rose flowers made of PDMS. The swelling is triggered in diisopropylamine and the de-swelling occurs in the open air.

Movie S6. Bi-directional and reversible morphing of a cup made of PDMS. The swelling is triggered in diisopropylamine and the de-swelling occurs in the open air.

Movie S7. Bi-directional and reversible morphing of frangipani flowers made of PDMS. The swelling is triggered in diisopropylamine and the de-swelling occurs in the open air.

Movie S8. Simulation and experiments of the morphing process of different pasta primitives during cooking. The final shapes range from 2D to 3D, from developable to non-developable geometries. The swelling was triggered in water at a temperature of 80 to 90 ℃ for three to 13 minutes. All the initial dimensions of the Frustum shaped grooves are 1.5 mm in the gap, 0.5 mm in width and 1.8 mm in depth.

REFERENCES AND NOTES

1. U.S. Environmental Protection Agency, (EPA), *Reducing Wasted Food & Packaging: A Guide for Food Services and Restaurants* (2015); https:// epa.gov/sites/production/files/2015-08/documents/reducing_wasted_food_pkg_tool.pdf. [the easiest access to this source is via the URL]
2. W. Wang, L. Yao, T. Zhang, C.-Y. Cheng, D. Levine, H. Ishii, Transformative Appetite: shape-changing food transforms from 2D to 3D by water interaction through cooking, in *Proceedings of the 2017 CHI Conference on Human Factors in Computing Systems* (ACM, New York, NY, USA, 2017), pp. 6123–6132.
3. Y. Tao, Y. Do, H. Yang, Y.-C. Lee, G. Wang, C. Mondoa, J. Cui, W. Wang, L. Yao, Morphlour: personalized flour-based morphing food induced by dehydration or hydration method, in *Proceedings of the 32nd Annual ACM Symposium on User Interface Software and Technology* (ACM, New York, NY, USA, 2019), pp. 329–340.
4. A. Sydney Gladman, E. A. Matsumoto, R. G. Nuzzo, L. Mahadevan, J. A. Lewis, Biomimetic 4D printing. *Nat. Mater.* **15**, 413–418 (2016).
5. Y. Kim, H. Yuk, R. Zhao, S. A. Chester, X. Zhao, Printing ferromagnetic domains for untethered fast-transforming soft materials. *Nature* **558**, 274–279 (2018).
6. R. M. Erb, J. S. Sander, R. Grisch, A. R. Studart, Self-shaping composites with programmable bioinspired microstructures. *Nat. Commun.* **4**, 1712 (2013).
7. T. van Manen, S. Janbaz, A. A. Zadpoor, Programming 2D/3D shape-shifting with hobbyist 3D printers. *Mater. Horiz.* **4**, 1064–1069 (2017).
8. H. Thérien-Aubin, Z. L. Wu, Z. Nie, E. Kumacheva, Multiple shape transformations of composite hydrogel sheets. *J. Am. Chem. Soc.* **135**, 4834–4839 (2013).
9. J. Kim, J. A. Hanna, M. Byun, C. D. Santangelo, R. C. Hayward, Designing responsive buckled surfaces by halftone gel lithography. *Science* **335**, 1201–1205 (2012).
10. J. Wu, Z. Zhao, X. Kuang, C. M. Hamel, D. Fang, H. J. Qi, Reversible shape change structures by grayscale pattern 4D printing. *Multifunct. Mater.* **1**, 015002 (2018).
11. L. Huang, R. Jiang, J. Wu, J. Song, H. Bai, B. Li, Q. Zhao, T. Xie, Ultrafast digital printing toward 4D shape changing materials. *Adv. Mater.* **29**, 1605390 (2017).
12. Y. Klein, E. Efrati, E. Sharon, Shaping of elastic sheets by prescription of non-Euclidean metrics. *Science* **315**, 1116–1120 (2007).

13. Q. Ge, C. K. Dunn, H. J. Qi, M. L. Dunn, Active origami by 4D printing. *Smart Mater. Struct.* **23**, 094007 (2014).
14. A. Cangialosi, C. K. Yoon, J. Liu, Q. Huang, J. Guo, T. D. Nguyen, D. H. Gracias, R. Schulman, DNA sequence–directed shape change of photopatterned hydrogels via high-degree swelling. *Science* **357**, 1126–1130 (2017).
15. E. Reyssat, L. Mahadevan, Hygromorphs: From pine cones to biomimetic bilayers. *J. R. Soc. Interface* **6**, 951–957 (2009).
16. M. M. Hamedi, V. E. Campbell, P. Rothemund, F. Güder, D. C. Christodouleas, J.-F. Bloch, G. M. Whitesides, Electrically activated paper actuators. *Adv. Funct. Mater.* **26**, 2446–2453 (2016).
17. Y. Liu, J. K. Boyles, J. Genzer, M. D. Dickey, Self-folding of polymer sheets using local light absorption. *Soft Matter* **8**, 1764–1769 (2012).
18. Z. L. Wu, M. Moshe, J. Greener, H. Therien-Aubin, Z. Nie, E. Sharon, E. Kumacheva, Three-dimensional shape transformations of hydrogel sheets induced by small-scale modulation of internal stresses. *Nat. Commun.* **4**, 1586 (2013).
19. J. Odent, S. Vanderstappen, A. Toncheva, E. Pichon, T. J. Wallin, K. Wang, R. F. Shepherd, P. Dubois, J.-M. Raquez, Hierarchical chemomechanical encoding of multi-responsive hydrogel actuators via 3D printing. *J. Mater. Chem. A* **7**, 15395–15403 (2019).
20. Z. Ji, C. Yan, B. Yu, X. Zhang, M. Cai, X. Jia, X. Wang, F. Zhou, 3d printing of hydrogel architectures with complex and controllable shape deformation. *Adv. Mater. Technol.* **4**, (2019), 1800713.
21. A. Lucantonio, P. Nardinocchi, L. Teresi, Transient analysis of swelling-induced large deformations in polymer gels. *J. Mech. Phys. Solids* **61**, 205–218 (2013).
22. M. Curatolo, P. Nardinocchi, E. Puntel, L. Teresi, Transient instabilities in the swelling dynamics of a hydrogel sphere. *J. Appl. Phys.* **122**, 145109 (2017).
23. H. Lee, J. Zhang, H. Jiang, N. X. Fang, Prescribed pattern transformation in swelling gel tubes by elastic instability. *Phys. Rev. Lett.* **108**, 214304 (2012).
24. Q. Li, Z. Xu, S. Ji, P. Lv, X. Li, W. Hong, H. Duan, Kinetics-induced morphing of three-dimensional-printed gel structures based on geometric asymmetry. *J. Appl. Mech.* **87**, 071008 (2020).
25. H.-B. Liu, H.-Q. Gong, Templateless prototyping of polydimethylsiloxane microfluidic structures using a pulsed CO_2 laser. *J. Micromech. Microeng*. **19**, 037002 (2009).

26. Y. Cao, R. Mezzenga, Design principles of food gels. *Nat. Food*. **1**, 106–118 (2020).
27. J. N. Lee, C. Park, G. M. Whitesides, Solvent compatibility of poly(dimethylsiloxane)-based microfluidic devices. *Anal. Chem.* **75**, 6544–6554 (2003).
28. Y. Hu, X. Chen, G. M. Whitesides, J. J. Vlassak, Z. Suo, Indentation of polydimethylsiloxane submerged in organic solvents. *J. Mater. Res.* **26**, 785–795 (2011).
29. D. P. Holmes, M. Roché, T. Sinha, H. A. Stone, Bending and twisting of soft materials by non-homogenous swelling. *Soft Matter* **7**, 5188–5193 (2011).
30. Y. Mao, L. Anand, A theory for fracture of polymeric gels. *J. Mech. Phys. Solids* **115**, 30–53 (2018).
31. S. A. Chester, C. V. Di Leo, L. Anand, A finite element implementation of a coupled diffusion-deformation theory for elastomeric gels. *Int. J. Solids Struct.* **52**, 1–18 (2015).
32. J. E. Dexter, R. R. Matsuo, B. C. Morgan, Spaghetti stickiness: Some factors influencing stickiness and relationship to other cooking quality characteristics. *J. Food Sci.* **48**, 1545–1551 (1983).
33. S. Nakamura, H. Satoh, K. Ohtsubo, Development of formulae for estimating amylose content, amylopectin chain length distribution, and resistant starch content based on the iodine absorption curve of rice starch. *Biosci. Biotechnol. Biochem.* **79**, 443–455 (2015).
34. H. M. Elmehdi, M. G. Scanlon, J. H. Page, M. I. P. Kovacs, Probing thermal transitions and structural properties of gluten proteins using ultrasound. *J. Ultrasound* **16**, 101–110 (2013).
35. M. Schirmer, M. Jekle, T. Becker, Starch gelatinization and its complexity for analysis. *Starch - Stärke*. **67**, 30–41 (2015).
36. Q. Zhang, J. Wommer, C. O'Rourke, J. Teitelman, Y. Tang, J. Robison, G. Lin, J. Yin, Origami and kirigami inspired self-folding for programming three-dimensional shape shifting of polymer sheets with light. *Extreme Mech. Lett.* **11**, 111–120 (2017).
37. Z. Chen, Q. Guo, C. Majidi, W. Chen, D. J. Srolovitz, M. P. Haataja, Nonlinear geometric effects in mechanical bistable morphing structures. *Phys. Rev. Lett.* **109**, 114302 (2012).
38. W. M. van Rees, E. Vouga, L. Mahadevan, Growth patterns for shape-shifting elastic bilayers. *Proc. Natl. Acad. Sci. U.S.A.* **114**, 11597–11602 (2017).
39. S. Armon, E. Efrati, R. Kupferman, E. Sharon, Geometry and mechanics in the opening of chiral seed pods. *Science* **333**, 1726–1730 (2011).
40. L. Levine, B. A. Drew, Rheological and Engineering Aspects of the Sheeting and Laminating of Doughs, in *Dough Rheology and Baked Product Texture*, H. Faridi, J. M. Faubion, Eds. (Springer, 1990), pp. 513–555.

41. R. Elbaum, L. Zaltzman, I. Burgert, P. Fratzl, The role of wheat awns in the seed dispersal unit. *Science* **316**, 884–886 (2007).
42. N. E. Stamp, Self-burial behaviour of erodium cicutarium seeds. *J. Ecol.* **72**, 611–620 (1984).
43. S. Sahin, S. G. Sumnu, Rheological properties of foods, in *Physical Properties of Food* (Springer, 2006), pp. 39–105.
44. B. J. Dobraszczyk, M. P. Morgenstern, Rheology and the breadmaking process. *J. Cereal Sci.* **38**, 229–245 (2003).
45. J. M. Faubion, R. C. Hoseney, The viscoelastic properties of wheat flour doughs, in *Dough Rheology and Baked Product Texture*, H. Faridi, J. M. Faubion, Eds. (Springer, 1990), pp. 29–66.
46. H. Zhu, A. Dhall, S. Mukherjee, A. K. Datta, A model for flow and deformation in unsaturated swelling porous media. *Transp. Porous Media*. **84**, 335–369 (2010).
47. A. Dorfmann, R. W. Ogden, Nonlinear electroelastic deformations. *J. Elast.* **82**, 99–127 (2006).
48. A. Logg, K.-A. Mardal, G. Wells, *Automated Solution of Differential Equations by the Finite Element Method: the FEniCS Book* (Springer, ed. 1, 2012), vol. 84.
49. R. G. M. van der Sman, M. B. J. Meinders, Prediction of the state diagram of starchwater mixtures using the Flory–Huggins free volume theory. *Soft Matter* **7**, 429–442 (2011).